Optimized design of a Linear Fresnel Reflector for solar process heat applications

Diego Pulido-Iparraguirre[1,2,3], Loreto Valenzuela[1,*], Juan-José Serrano-Aguilera[4], Aránzazu Fernández-García[1]

[1] CIEMAT, Plataforma Solar de Almería, Crta. Senés, km. 4.5, E04200, Tabernas, Almería, Spain

[2] Universidad de Antofagasta, Avenida Angamos, 601, Antofagasta, Chile

[3] Universidad de Almería, Crta. De Sacramento s/n, E04120, La Cañada de San Urbano, Almería, Spain.

[4] Universidad de Málaga, Escuela de Ingenierías Industriales, Campus de Teatinos s/n, 29071, Málaga, Spain

Abstract

Heat demands in industrial processes represent a high rate of the thermal energy consumption that could be directly delivered by a concentrated solar thermal technology. Linear Fresnel reflectors are a promising example of this kind of technology. This paper presents an innovative and optically optimized design of linear Fresnel collector for solar process heat applications. An in-house ray trace code was employed to evaluate different geometrical options of the solar collector over conventional concepts, aiming to maximize its optical performance and tackle the inherent weakness of this concentrating solar technology when it is compared to other type of concentrators. Geometrical modifications accomplished in the optimization process include the tilt of the concentrator and receiver, the receiver displacement and the concentrator rotation along with the optimization of other relevant parameters. As a result, a significant upgrade of the monthly power on the receiver was achieved, with an average enhancement ranging from 2% to 61%, compared to a standard linear Fresnel collector without the proposed modifications. This result provides a more homogenous thermal power profile delivered along the year, which is an important requirement to place the technology in the spotlight.

Keywords: concentrating solar thermal technology, linear Fresnel reflector, ray trace code, optimized optical performance, incidence angle.

Nomenclature

Acronyms

CPC	compound parabolic concentrator
CSR	circumsolar ratio
DNI	direct normal irradiance
DSG	direct steam generation
IAM	incidence angle modifier
LFR	linear Fresnel reflector

* Corresponding author: Loreto Valenzuela; e-mail address: loreto.valenzuela@psa.es; Phone: 0034 950387934; Fax: 0034 950365015

NAP	normalized accumulated power
O&M	operation and maintenance
PTC	parabolic-trough collector
RTC	ray trace code

Symbols

$\dot{Q}_i$	internal power of the fluid (W)
$\dot{Q}_r$	power transferred to the fluid (W)
$\eta_{opt,0^\circ}$	peak optical efficiency of the LFR
η_{opt}	optical efficiency of the LFR
μ	mean value of the gaussian distribution (rad)
A	transversal area of the tube (m^2)
Cp	specific heat capacity of the fluid (kJ/kg·K)
D	inner diameter of the tube (m)
dz	receiver displacement (m)
$\tilde{G}_{b,a}$	solar irradiance impinging in the absorber (W/m)
H	receiver height (m)
L	length of the receiver (m)
m	flow rate (kg/s)
Re	Reynolds dimensionless number
v	velocity of the fluid (m/s)
β	east-west concentrator rotation angle (º)
γ	tracking angle (º)
ΔT	temperature gain of the fluid (K)
η	overall efficiency
θ	angle of incidence (º)
θ_L	longitudinal angle of incidence (º)
θ_T	transversal angle of incidence (º)
λ	tilt angle of the reflectors and receiver (º)
ν	kinematic viscosity of the fluid (m^2/s)
ρ	density of the fluid (kg/m^3)
σ	standard deviation of the Gaussian distribution (rad)
ϕ	Buie's sunshape profile
ϑ	angular spherical coordinate
φ	azimuthal spherical coordinate
χ	circumsolar ratio
γ	Buie's sunshape variable
κ	Buie's sunshape variable
F	cumulative distribution function
$\hat{\mathrm{X}}$	sequence of uniformly distributed random numbers
$\vec{v}_i$	unitary vector pointing at the incoming ray direction
$\vec{v}_r$	direction of the reflected ray
$\vec{n}$	normal vector to the mirror surface

Subscripts

opt	optimum
set	set
0	zero
ss	relative to sunshape

er	relative to the Gaussian distribution modeling errors of mirrors surface	*max*	maximum

1. Introduction

World energy consumption has constantly increased over the past century, mostly related with the electricity and petroleum derivatives demand (IEA 2016). One of the main reasons to move from fossil fuels to renewable energies, and in particular to solar energy, is the indisputable climate change which is causing the major environmental problem worldwide faced so far (Azofra et al. 2014). This issue has promoted international agreements against pollution (European Comission 2017) altogether with tax reduction or subsidies for those who comply with the regulations (REN21 2016). In addition, renewable energies present an economic certainty in contrast to the instability of fossil fuel price, due to limitations in supply capacity alongside its dependence on the international scenario along the lifetime of operation (Corona et al. 2016).

Industries, including both those related to the procurement of goods and products and indirect uses through cogeneration, consume nearly 30% of the total energy demanded worldwide (IEA 2016). Industrial processes require thermal energy in several temperature ranges. In order to specify which solar technology fits to a given process, it is useful to identify its temperature level (Vannoni, Tobergte, and Curtis 2013). For the purpose of this work, attention is paid to processes in the range of temperatures between 100 °C and 400 °C. About 30 % of the total industrial heat demanded is required at temperatures below 100 °C and 27% at temperatures below 400 °C (Werner and Constantinescu 2006). Other applications that require thermal energy in this temperature range are desalination (García-Rodríguez and Blanco-Gálvez 2007), refrigeration by double effect absorption chillers (Tierney 2007) or electricity production through organic Rankine cycles (Freeman, Hellgardt, and Markides 2015). Certainly, this is a significant rate of thermal energy consumption that could be directly supply by a concentrated solar thermal technology.

The solar technology suitable for these temperatures is linear focusing collectors, i.e., parabolic-trough collectors (PTCs) and linear Fresnel reflectors (LFRs). It has been found that LFR technology presents some significant advantages compared with PTC (Sahoo, Singh, and Banerjee 2012; Sait et al. 2015). First, the costs of the optical components are lower in LFR, according to the nearly flat shape of the mirrors (Boito and Grena 2016) and also to the absence of metal-glass welds in the receiver tubes, because in most of the designs the receiver tubes are partially covered with a secondary reflector and the need of an evacuated atmosphere around the receiver is not considered. Although, it is worth to mention that the metal-glass welds commented above are not commonly incorporated to PTCs typically designed for low temperature process application near 200 ºC, which use non-evacuated glass-enveloped tubes (Millioud and Dreyer 2008; NEP Solar 2018). In addition, as the receiver in LFR is fixed (contrarily to the case of PTC), it does not use flexible hoses or ball joints between adjacent collectors at the points where the distribution pipe meets the start and end of the collector. As a consequence, lower operation and maintenance (O&M) costs for LFR plants are required (Häberle et al. 2002). On the other hand, the main disadvantage of LFR compared with PTC, is the lower optical efficiency, explained by the

transversal component of the radiation impinging the receiver tubes, which increases when the Sun is far away from the zenithal position. In a lower level, slight optical errors due to the larger distance between the mirrors and the focal point contribute to decrease the optical performance (Abbas 2017; Abbas et al. 2013).

LFR is compiled of an array of flat or nearly flat primary reflectors and a receiver. The primary reflectors track the Sun along the daytime reflecting the direct solar beams. The rays reflected impinge on the receiver, which remain fixed. The energy absorbed by the receiver is transferred to the working fluid flowing through it. Due to the fact that the total area of the primary reflectors is larger than the area of the receiver that collects the reflected radiation, the concentration phenomenon takes place proportionally to the rate of these two areas (Qiu et al. 2015).

A small group of LFR's designs oriented to work in the range of temperature required by industrial processes has been developed and main characteristics and performance results published. Among those designs, the one accomplished by the German company Industrial Solar (lately named PSE AG) (Häberle et al. 2006) has been used in several emblematic projects, as the solar/gas cooling plant at the Engineering School of Seville (Spain) (Bermejo, Pino, and Rosa 2010). This facility provides the 75% of the energy feeding a double-effect LiBr + water absorption chiller of 174 kW nominal cooling capacity. Other initiative that uses the Industrial Solar collector is the commercial direct steam generation (DSG) project constructed in Jordan (M. Mokhtar et al. 2015) to provide saturated steam for process heat. The design mentioned consists of a standard conception with slightly curve mirrors tracking the Sun, while the receiver is integrated by an evacuated receiver tube model PTR® 70 by SCHOTT and a secondary compound parabolic concentrator (CPC) made of aluminum reflectors. Both the receiver and the reflector are in individual horizontal planes and the collector is north-south oriented.

Another LFR that is worth mentioning, is the one accomplished by the Spanish company Inersur (Inersur 2017) which provides the energy required in a local slaughterhouse. Although the design does not present any particular innovation, it is one of the few commercial projects for industrial processes currently on operation. One additional interesting development come from a Spanish company named Solatom (Solatom 2017). This design presents an improvement consisting on an easy-mounting and easy-transport collector which is integrated in a container able to be placed in the required facilities, by unfolding the lateral walls to give place to the structure of the LFR. There are also a few prototypes under development, whose purpose is more focused on the validation of mathematical models than devoted to commercial systems (G. Mokhtar, Boussad, and Noureddine 2016; Wang et al. 2017; Y. Zhu et al. 2017).

Most of the above mentioned projects are part of the group of standard and conventional designs from the optical point of view. This brings as a consequence the existence of persistent disadvantages concerning the optical performance: (a) variability of the energy production along the day and year due to the relative position of the Sun related to the reflection surface; (b) energy production decrease for locations far away from the equator; (c) reduction in the effective surface of reflection due to blocking and shadows.

Some prototypes can be found on the literature that incorporates certain geometrical modifications oriented to enhance the optical behavior of the collector. Dai describes three simultaneous types of movements: the elementary of the mirrors tracking the Sun, east-west translation of the entire reflector

field according to the relative position of the Sun, and rotation of a secondary reflector located in the receiver (Dai et al. 2012). Zhu proposes a design east-west oriented, which has the possibility to adjust the tilt of the entire collector, agreeing to the solar height (Y. Zhu et al. 2017). Also, Zhu shows another prototype with east-west orientation, including both a reflective surface that forms a parabola and a receiver, which is able to move along the axial axis to compensate the end losses (Yanqing et al. 2016). This last modification is also proposed by Barbon (Barbon, A., Barbon, N., Bayon 2016). Finally, Nixon presents a design that allows mirrors to individually rise and descend on the horizontal plane (Nixon and Davies 2016). It is important to note that in all the cases mentioned above, geometric modifications with respect to the conventional design of LFR are applied individually. However, the design presented in this work combines simultaneously several of the previous modifications, as well as integrates some innovative improvements.

One of the main approaches to boost this technology is to improve the optical efficiency but avoiding a significant increase in the final costs. Following this purpose, this study is focused on the development of an innovative LFR design, aiming to compensates, as much as possible, the optical weakness inherent to the LFR technology. The optical parameters were evaluated and optimized through the use of an optical model performed by an in-house ray trace code (RTC). Numerical results of the increase of performance achieved are presented.

2. Methodology

This section includes the steps followed, in the present work, to simulate the optical behavior of the LFR with the aim of optimizing its performance.

2.1 Ray trace code description

The implementation of an in-house RTC is relevant at the time of carrying out optimization procedures, which entails a vast number of optical simulations for the different geometrical parameters describing the arrangement of the optical system in the LFR. In this work, a trade-off approach was followed to achieve an efficient code from the computational point of view, whereas accurate results are needed to select the optimum optical configuration resulting from a global optimization task. The flowsheet of the code is shown in Fig. 1.

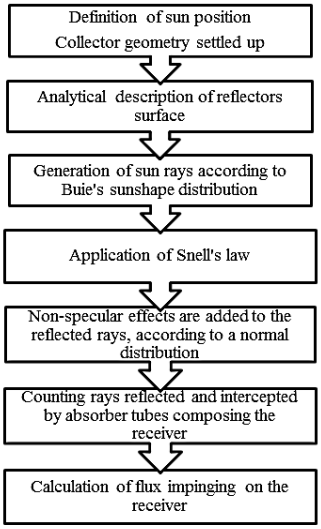

Fig. 1. Flowsheet scheme of in-house ray trace code.

A three-dimensional model (developed in the Matlab® software environment) based on a stochastic approach was followed, where the sunshape distribution concerning the direction of the incoming solar rays is taken into account by means of the Buie's sunshape profile (ϕ), (Buie, Monger, and Dey 2003; Buie, Dey, and Bosi 2003), equations (1) and (2), with a constant circumsolar ratio (CSR) value of 0.2

$$\phi(\vartheta) = \begin{cases} \dfrac{\cos(0.326\vartheta_{ss})}{\cos(0.308\vartheta_{ss})} & \text{for } \ 0 \le \vartheta_{ss} \le 4.65\ mrad, \\ e^{\kappa}{\vartheta_{ss}}^{\gamma} & \text{for } \ \vartheta_{ss} > 4.65\ mrad \end{cases} \tag{1}$$

where γ and κ are two parameters which depend on the circumsolar ratio, χ defined.

$$\begin{aligned} \gamma &= 2.2\ln(0.52\chi)\,\chi^{0.43} - 0.1 \\ \kappa &= 0.9\ln(13.5\chi)\,\chi^{-0.3} \end{aligned} \tag{2}$$

The equation (3) describes the percentage of the solar energy content in the solar disk, depending on the angular displacement in spherical coordinates (ϑ and φ):

$$F_{ss}(\vartheta_{ss}) = \frac{\int_0^{2\pi}\int_0^{\vartheta_{ss}} \phi(\vartheta)\sin(\vartheta)d\vartheta d\varphi}{\int_0^{2\pi}\int_0^{\vartheta_{max}} \phi(\vartheta)\sin(\vartheta)d\vartheta d\varphi} \tag{3}$$

where F_{ss} is the cumulated distribution function of the rays according to Buie's sunshape. ϑ_{ss} is the radial angle value associated to each ray and ϑ_{max} stands for the radial extent of the sun (i.e. solar disk and the whole sun aureole).

Monte Carlo method was used to generate the initial bunch of rays before reaching the reflector surface. It defines the position of the initial ray within the aperture plane along with its direction according to the sunshape profile, which in turns include the radial angle of the ray respect to the sun position. To feed the Monte Carlo algorithm, a uniformly distributed random sequence of numbers was generated. Particularly the *Mersenne Twister* algorithm (Matsumoto and Nishimura 1998) was applied to generate all the incoming rays. The code was implemented aiming to reproduce the pattern of emitting power within the solar disk. It means that the radial angle value associated to each ray follows a particular probability distribution related to the aforementioned sunshape profile, allocating to each ray the same amount of

radiant energy.

Monte Carlo methods evaluate the inverse of the cumulative distribution function (F_{ss}^{-1}) from a uniformly distributed random sequence of numbers so that $0 < \hat{X} < 1$. Provided that the same amount of power is associated to each ray and the sunshape distribution is axial-symmetric, the obtained sequence of angles ($\hat{\vartheta}_{ss}$) reproduces the sun sunshape profile. The azimuthal angle φ is equidistributed from 0 to 2π and ϑ depends on the sunshape according to the equation (4):

$$F_{ss}^{-1}(\hat{X}) = \hat{\vartheta}_{ss} \tag{4}$$

Some assumptions from geometric optics were imposed to trace the path of rays in the air, where atmospheric extinction is neglected due to the short distances between the primary reflectors and the receiver. According to the particular position and tilt of mirrors, the path of the incoming rays is checked in case of shadows induced by adjacent mirrors prior to reflection. The primary mirrors considered are silvered glass type. In this case, Snell's Law is applied to model specular reflection without taking into account effects of refraction at the interface of glass layer on mirrors. As detailed in equation (5), the normal vector to the mirror surface is $\vec{n}$ whereas $\vec{v}_i$ stands for the unitary vector pointing at the incoming ray direction and $\vec{v}_r$ to the respective direction of the reflected ray.

$$\vec{v}_r = 2(\vec{v}_i \cdot \vec{n})\vec{n} - \vec{v}_i \tag{5}$$

Non-specular effects should be included when addressing reflection, under realistic working conditions. These effects are mainly the consequence of small-scale slope errors (surface waviness) on the mirror surface as well as reflector geometrical errors (Güven and Bannerot 1986). To model such sort of phenomena, the reflected vector was deviated a particular angle. The determination of this angle, $\hat{\vartheta}_{er}$, of radial deviation is performed by means of a stochastic algorithm, according to equation (6). The non-specular deviation of the energy reflected was considered as a normal distribution with null mean value (μ=0 mrad) and a characteristic standard deviation (σ_{er}=0.002 mrad). The implemented model, takes advantage of the analytical-defined description of the geometry of each mirror.

$$\hat{\vartheta}_{er} = F_{ss}^{-1}(\hat{X}) = \sqrt{-2\sigma_{er}^2 \ln(1 - \hat{X})} \tag{6}$$

This asset enables a fast computation of the local normal vector to the reflector surface as well as the reflection point corresponding to each ray.

The trajectory of the reflected rays is checked to detect blockage by adjacent reflectors. Also, the intersection of the straight lines representing the rays' path with the 3D surface describing the neighbor mirrors is calculated. The analytical description of the reflector surface makes it possible to obtain such intersection points efficiently. As a result, blocked rays are ruled out. The intersection of the reflected rays with the receiver, which was selected as a multitube configuration (as described in section 3.2.1), is also based on the analytical description of each absorber tube as a cylinder (bounded in the axial direction). This final set of intersection points is used to work out the concluding histogram which in turns provides the concentrated flux distribution on each absorber tube of the receiver.

It is worth mentioning that this sort of problem can be solved partially as a consequence of the

superposition principle. Having on goal the implementation of a modular code which is capable of working in memory-limited computers, the RTC algorithm is launched for each mirror, where the particular concentrated flux profile of each absorber tube is calculated based on the solar rays reflected by a single mirror. The final concentrated solar irradiance profile for each absorber tube is the result of overlaying the contribution of all the mirror facets in the system. At the same time, the overall optical efficiency of the system can be found from a relatively reduced number of rays launched by the algorithm, what enables a suitable tool (fast code) to seek the optical arrangement which maximizes the optical efficiency of the systems for a specific position of the sun. In line with this, a three-dimensional modeling of the optical system is essential to analyze all the relevant effects and particular features of the innovative system under study.

Several simulations were done with the RTC described to achieve an optimized design of a LFR. As reference case, the code was run by using the meteorological data and the Sun position of the *Plataforma Solar de Almería* (Almería, southern Spain). The data from a meteorological year were utilized, sampling the average direct normal irradiance (DNI) every five minutes for the 365 days of the year. The objective of these simulations was to maximize the energy impinging on the receiver along the year, and the geometry of the LFR that achieves this maximum was selected as the optimal design.

2.1.1 Ray trace code validation

The results accomplished by the in-house RTC were contrasted with trustworthy ray trace software in order to confirm that every phase of the RTC is correct. The selected control software is Tonatiuh, a simulation tool aiming to create an open source, cutting-edge, accurate, and easy to use Monte Carlo ray trace for the optical simulation of solar concentrating systems (Blanco et al. 2009). This software is still being developed by the National Renewable Energy Centre of Spain (CENER) with the former collaboration of the University of Texas at Brownsville (UTB), and the support of the National Renewable Energy Laboratory (NREL).

A simulation was carried out using the same environment parameters and collector geometry. The comparison is done with the results of the flux density in each tube of the receiver, considering a configuration of the receiver integrated by six parallels absorber tubes.

For the sake of a clearest explanation, only one tube out of the six has been presented (Fig 2). The flux density is showed in four different perspectives, in order to highlight the optimum agreement in the whole tube. The top image of each view responds to the in-house RTC and the bottom image to Tonatiuh software. Four views of the flux density in the receiver tube are showed in Fig.2. Top left picture is the isometric perspective of the flux, while in the top right box a lateral view of the flux in the tube can be seen, highlighting how precise is the match between both simulations. In the bottom left box, the up view of the flux in the tube is presented, and finally the front perspective of the flux in the angular position appears on the bottom right box. There is a satisfactory match in terms of flux density values and the distribution of the flux across the tube between both simulation tools. Even so, it is significant that the in-house RTC achieve a smoother shape than Tonatiuh, with smaller amount of rays and fewer computing time.

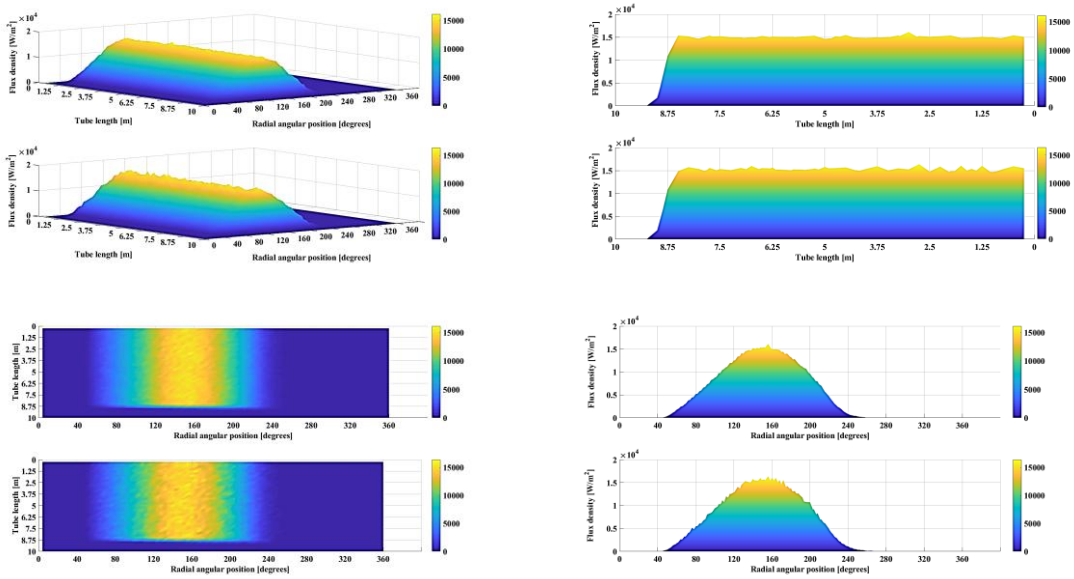

Fig. 2. Comparison between two simulation tools, Tonatiuh (top) and in-house RTC (bottom). Top left: isometric view. Top right: lateral view. Bottom left: up view. Bottom right: front view.

2.2 Optimization of the LFR components

It is worth emphasizing the components of the LFR that are relevant in the operation. They are the concentrator and the receiver. The design procedure together with technical approached adopted is presented in this section.

2.2.1 Concentrator design

This section comprises a description of the methodology accomplished to select and design the optical concentrator of the LFR, focusing on the shape, number and width of mirrors as well as the tilt and rotation of the concentrator.

Before detailing the different steps followed to optimize the LFR it is worth mentioning that the optical efficiency of a tracking solar collector and in particular of a LFR varies with the sun position. For this Collector design, it is function of the incidence angle, including both components: longitudinal and transversal (G. Zhu 2013). The incidence angle modifier (IAM) depends also on both components of the incidence angle and modifies the optical efficiency as follows:

$$\eta_{opt}(\theta_T, \theta_L) = \eta_{opt,0^\circ} \cdot IAM(\theta_T, \theta_L) \tag{7}$$

where $\eta_{opt,0^\circ}$is the peak optical efficiency of the LFR that depends on the optical parameters (reflectance, transmittance, absorptance and intercept factor of the components of the LFR) and the IAM can be factorized into two individual functions for computational convenience ($IAM(\theta_T, \theta_L) \cong IAM(\theta_T) \cdot IAM(\theta_L)$). In PTC, the transversal component of the incidence angle is 0° or quite close to 0° because the receiver rotates with the concentrator, which makes $IAM(\theta_T)$ to be 1 or close to 1 in this type of solar tracking collectors. However, in the case of LFR collectors, the transversal component vary along the day, what reduces the optical efficiency of LFRs compared to PTCs.

A comparison of the IAM between a standard LFR configuration and the one with the improvements

proposed in the following sections was carried out. By varying the transversal component of the sun position related with azimuth angle from sunrise (90º) to sunset (270º) and longitudinal component attached to zenith angle (0º in the zenith), the power impinging in receiver was obtained for every possible combination of both angles. Later, all values were normalized resulting in the global IAM.

2.2.1.1 Shape of primary mirrors

With respect to the primary reflectors, flat, parabolic and cylindrical shapes were analyzed. The image reflected by flat mirrors on the receiver is slightly wider than the mirror width due to the sunshape effect. However, in this specific case it is approximately equivalent because the distance traveled by the reflected rays from the mirrors to the receiver is quite small (only few meters) and consequently the final width of the image at the receiver surface will not be considerably increased. For this reason, the optimal width for flat shaped mirrors should be nearby to the width of the receiver. If this condition was not established and wider mirrors were used, the reflected image would certainly be wider than the receiver and several rays will miss the target, which is known as an overflow effect. It is worth highlighting here that flat mirrors do not concentrate solar radiation by themselves, since the reflecting surface area is the same as the receiving area. In this case the concentration is achieved by the group of mirrors aiming to the same point.

In case of using parabolic mirrors, the image reflected tends to converge to the focal point of the parabola, reflecting a beam of rays whose width is lower than the receiver width. In order to increase the power impinging on the receiver, wider mirrors could be considered without the limitation found in flat shaped mirrors. Wider mirrors imply more solar radiation collected in the reflector aperture, which leads to raise the concentration factor of the LFR. In addition, the height of the receiver over the lines of mirrors must be adjusted in order to fit the image reflected to the target.

Cylindrical shaped mirrors, which present quite similar optical behavior to parabolic shaped mirrors, are a suitable alternative solution from a practical and economical perspective because they involve an easier and cheaper manufacturing process. The main characteristic of cylindrical mirrors is the radius of curvature, which is twice the focal length of parabolic shaped mirrors for the same receiver height (Abbas, Muñoz, and Martínez-Val 2012). A higher radius of curvature involves a smoother geometrical profile, which entails a significant advantage for the manufacturing of the concentrator because it may be accomplished with thin glass mirrors glued over a cylindrical preformed pattern, which is quite feasible to achieve. In this work, several simulations were accomplished to compare the power impinging on the receiver for flat, parabolic and cylindrical alternatives.

2.2.1.2 Number and width of mirrors

Having on goal the collection of the maximum power in the receiver, the selection of the number and width of mirrors is not a trivial issue. More and wider mirrors imply a larger reflecting surface, which leads to higher rate of solar radiation collected in the aperture of the LFR. As a consequence, the power maximization cannot be the only design criterion to find the optimum number and width of mirrors. An economical approach combined with practical and technical aspects of the industrial facility, where this system will be installed, is the best strategy to follow. For example, each mirror configuration involves an optimum receiver height, which must be suitable for the facility characteristics as well. Consequently,

these two parameters could be selected for every specific demand using the RTC developed in this work.

2.2.1.3 Concentrator tilt

A significant innovation, from the optical point of view, presented in this work in comparison with traditional reflectors is that the plane containing the axial axes of the mirrors is not parallel to the horizontal plane, in contrast to conventional linear Fresnel systems available. The tilt in the north-south direction is defined by the angle λ, represented in Figure 1. This tilt noticeably reduced the optical losses due to the longitudinal angle of incidence, θ_L, which is the angle that forms the longitudinal component of the Sun's rays with the normal to the plane of the collector aperture. This angle depends on the relative position of the Sun with respect to the collector and thus it is a function of the location, time and day (Huang, Li, and Huang 2014). An additional advantage provided by the reflectors tilt, is that the path of the reflected rays that imping on the receiver is shorter compared with the path of reflected rays from horizontal reflectors. Consequently, the dispersion phenomenon of the rays because of the sunshape distribution and the scattering effect on the mirrors is reduced. Altogether with the fact that the density of energy contained in the rays bundle increases thanks to the shorter path of the rays. Therefore, the optimum tilt was calculated to minimize the annual optical losses for each location (i.e., it depends on latitude). Nevertheless, due to technical limitations, such as accessibility and cost of the structure, it is advisable to establish a trade-off solution.

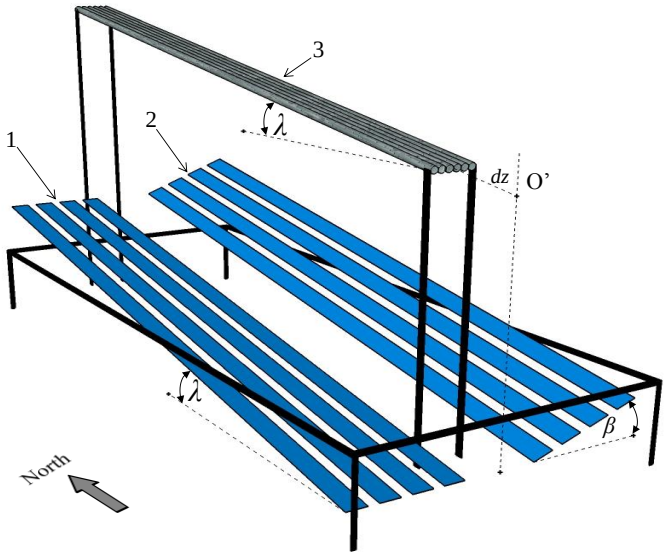

Fig. 3. General scheme of the optimized LFR.
1: West reflector surface. 2: East reflector surface. 3: Receiver. λ: tilt angle of the reflectors and receiver. β: angle of the east-west rotation. *dz*: receiver displacement

It is also important to remark that the axial axis of the absorber tubes must always be parallel to the axes of rotation of the reflector, which means that the receiver is also tilted an angle equal to λ. In this sense, the distance between an individual mirror and the receiver remains constant along the longitudinal axes of the collector. This is a condition imposed by the fact that the tracking angle, γ, of each mirror depends on the distance between the mirror and the receiver and, consequently, if this distance was not constant it would be necessary to have different γ for each single mirror at the same time, which is a very difficult task to accomplish in the practice.

2.2.1.4 Concentrator rotation

The set of reflectors is composed of an even number of them, in such a way that half are located at the east of the receiver while the other half are located in the west side, and both sets are supported by two separate structures. Each reflector has an independent tracking control on a single axis (which is the same as the axial axis of the reflector) to follow the Sun along the day, whose degree of freedom is the tracking angle, γ (see Fig. 4). In conventional LFRs these tracking axes are contained in the horizontal plane.

In this design, each set of mirrors are able to individually rotate with respect to the central axis of the concentrator, with an angle β named as the east-west concentrator rotation angle (see Fig. 4 and 5). The angle β of the east set of reflectors (β_{east}) is not linked to the angle of the west group (β_{west}), so their drives are independent. The independency of movement between the two sets of reflectors responds to the Sun position, i.e., if the Sun is on the west side of the receiver only the east set of reflectors starts to rotate into angle $\beta_{east} > 0$ while the east side stay in the position in which $\beta_{west} = 0$ (see Fig. 4).

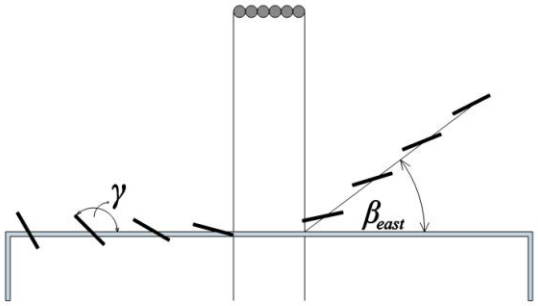

Fig. 4. Representation of angles β and γ in the transversal plane of the collector.

The rotation of each set of mirrors according to the angle β involves two different enhancements in terms of optical performance. First, it reduces the cosine factor, which is due to the transversal incidence angle, θ_T, formed by the transversal component of the incidence rays, I, and normal vector of the reflector surface, n (see Fig. 5). The former is due to the inclination adopted by the reflectors when the set of them has rotated in an angle $\beta > 0$ (γ_b in Fig. 5), compared with the inclination if there had not been rotation at all (γ_a in Fig. 5). For an identical Sun position, the angle θ_T differs in the two cases ($\theta_{T,a}$ and $\theta_{T,b}$), being smaller when a $\beta > 0$ is adopted (that is, $\theta_{T,b} < \theta_{T,a}$), which implies a higher optical efficiency. Secondly, the effect of blocks and shadows by neighboring reflectors is attenuated thanks to this rotation. As a consequence, the power impinging on the receiver away from the solar noon is higher than in conventional LFRs. In this way, the daily distribution of thermal power production is more homogeneous and does not drastically decay out of the solar noon. Similarly to the effect found with the concentrator tilt (i.e. λ angle), the rotation of the concentrator through the β angle leads to a narrower path of the reflected rays, which is positive in terms of system's optical efficiency.

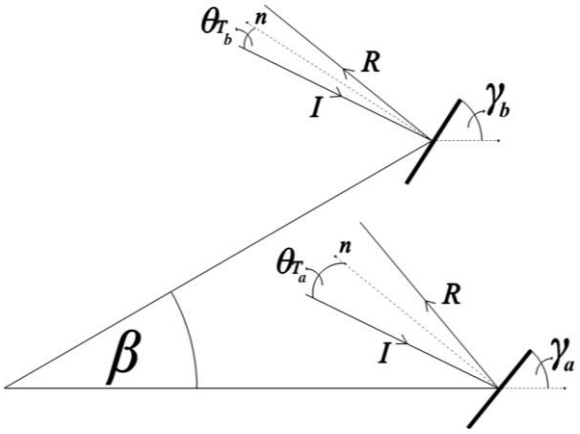

Fig. 5. Representation of the influence of β angle in θ_T.

2.2.2 Receiver design

This section includes the guidelines followed to select the receiver configuration along with the description of the different steps devoted to find the optimal point strategy, the height of the receiver, the axial displacement of the receiver and the criterion adopted to determinate the length of the collector.

2.2.2.1 Receiver configuration

The methodology applied to select the proper receiver configuration consisted on performing a thorough literature revision to analyze the advantages and disadvantages of the two main existing designs. A considerable number of the LFR designs agreed in using a receiver composed by a single tube with a secondary reflector (Selig 2011; Bernhard, Laabs, and Lalaing 2008) (see Fig. 6 left). Some of the largest LFR thermal plants employ this configuration (Morin et al. 2011). This design could be conceived with a second glass tube surrounding the metal one and vacuum between them, or just a single steel tube with a flat glass cover closing the secondary reflector cavity and sealing the receiver from outside weathering conditions (Montes et al. 2016).

On the other hand, other designs conceive an innovative approach based on a trapezoidal cavity with a multitube absorber (see Fig. 6 right). This design includes an array of parallels tubes. The target area of the multitube receiver is considerably larger than the area of the single tube receiver. This leads to enhance the possibility of an incoming ray to imping on the desired tubes without a second reflection. However, the former characteristics of the multitube receiver leads to a lower concentration ratio compared to single tube receiver. Regarding the additional reflection taking place in the secondary reflector of the single tube concept, this phenomenon decreases the energy in the reflected rays due to the energy absorption of the secondary mirror. The main advantages of trapezoidal cavity with multitube absorber are a higher efficiency in the optical and thermal process and a more flexible design leading to simpler control of the flow through the tubes (Abbas, Muñoz, and Martínez-Val 2012).

In both configurations the upper and laterals walls are thermally insulated to avoid heat losses (see Figure 6 item 1). In this configuration the absorber tube or tubes are covered by the cavity and consequently a thermocline phenomenon of the air is promoted. The glass cover (see Figure 6 item 5) is facing down and so the glass allows the incoming radiation passing through it and imping in the tubes, while minimize the convection heat losses from the inside of the receiver to the exterior, causing a greenhouse effect.

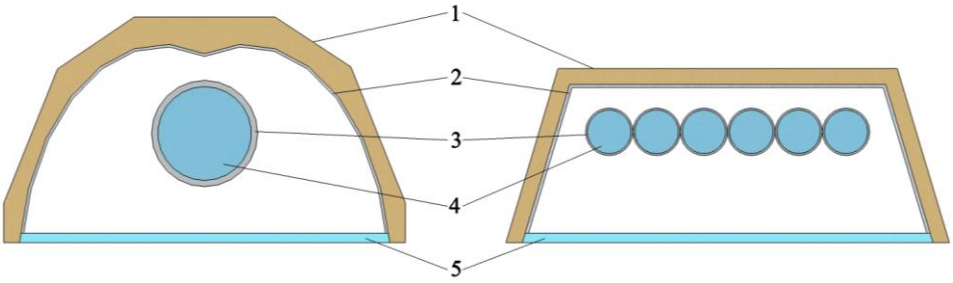

Fig. 6. Receiver configuration. Left: Single tube with secondary reflector. Right: Trapezoidal cavity with multitube absorber. 1: Isolation recovery. 2: Secondary reflective surface. 3: Steel tube. 4: Working fluid. 5: flat glass cover.

2.2.2.2 Length of the reflectors and the receiver tubes

To calculate the length of each LFR unit, and consequently of the receiver length, a thermal balance was performed in Matlab® environment, having on goal a high Reynolds number, equation (8), to assure there is turbulent flow inside the absorber tubes.

$$Re = v \cdot D/\nu \tag{8}$$

where Re is Reynolds dimensionless number, v is the velocity of the fluid in (m/s), D is the inner diameter of the tube in (m) and ν is the kinematic viscosity of the fluid in (m^2/s).

Later the flow rate of the fluid is determinate by equation (9):

$$\dot{m} = v \cdot \rho \cdot A \tag{9}$$

where $\dot{m}$ is the flow rate in (kg/s), ρ is the density of the fluid in (kg/m^3) and A is the transversal area of the tube in (m^2).

Finally, the thermal balance, equation (10), was accomplished by matching the internal power ($\dot{Q}_i$) gained, considering the increment of temperature previously set, and the power transferred to the fluid ($\dot{Q}_r$) through the tube walls, coming from the impinging radiation in the absorber.

$$\begin{gathered} \dot{Q}_i = \dot{m} \cdot c_p \cdot \Delta T \\ \dot{Q}_r = \tilde{G}_{b,a} \cdot \eta \cdot L \\ \dot{Q}_i = \dot{Q}_r \end{gathered} \tag{10}$$

where $\dot{Q}_i$ is the internal power of the fluid in (W), c_p is the specific heat capacity of the fluid in (kJ/kg/K) and ΔT is the temperature gain of the fluid in (K). $\dot{Q}_r$ is the power transferred to the fluid in (W), $\tilde{G}_{b,a}$ is the solar irradiance impinging in the absorber (delivered by the RTC) per unit length of receiver in (W/m), η is the overall efficiency and L is the length of the receiver necessary to collect the power/energy that yield in the temperature gain previously established.

An increase of 20 ºC in the temperature of the heat transfer fluid (in this case pressurized water) was set as the second criterion to determine the length. This thermal gain was imposed to minimize the

temperature relative errors when carrying out the experimental test campaign to characterize the thermal performance of the LFR prototype. The accuracy of the measurement instruments was also considered at the time of setting the temperature difference in the LFR.

2.2.2.3 Point strategy

Considering the transversal plane of the receiver, the image formed by reflected rays has a significant relevance in the overall performance of LFR. Due to the fact that this particular receiver is not a singular aiming point, but a group of tubes, every tube should be irradiated homogeneously. This means that a homogeneous solar flux should be maintained so that hot spots, which could lead to thermal stress in the tube material, can be avoided. Two point strategies were analyzed with the in-house RTC simulation to address this issue along with the concentration ratio.

2.2.2.4 Receiver height

The distance from the mirrors plane to the receiver, *H*, was established by maximizing the power delivered to the receiver. A set of calculations for different receiver heights, fixing the rest of parameters and derived from the corresponding focal length, was carried out to study the relationship among the different geometrical parameters and to find the combination that yields an optimum receiver height, H_{opt}. Additionally, a stochastic approach was included in the model simulating the deviation of rays caused by mirrors aberrations. The longer distance traveled by the rays, the more manifest this phenomenon is.

2.2.2.5 Receiver axial displacement

A key headway in relation to the setting of the receiver consists on moving northward the absorber tubes a certain distance, *dz*, (see Fig. 3) in the same direction as the marked by their axial axis. This axial displacement is defined from an origin (*O'* in Fig. 3), which is the point of intersection between the axial axis of the absorber tubes and a plane perpendicular to these axes, which cut to the reflectors plane at its southern end. This shift allows a significant reduction of the geometrical collector end losses. As the solar rays are coming from the south most of the year, they are reflected with northern component and cannot be absorbed by the receiver north end, as a result of its finite length. The design considers a fixed displacement to tackle this issue, avoiding moving devices to change the displacement *dz* according to the Sun position, which would entail a higher cost. This implies that the optimal value for the parameter, dz_{opt}, is the result of a global optimization process performed with the RTC and ensures constructive simplicity of the receiver bracket.

3. Results

This section presents the results of the simulation carried on by the Monte Carlo RTC with the aim of maximizing the energy impinging on the receiver along the year. These simulations deliver the optimal value of the variable inquired that achieves this maximum, such as the tilt of the concentrator and receiver, λ_{opt}, the east-west concentrator rotation, β_{opt}, the height of the receiver, H_{opt}, , and the receiver displacement, dz_{opt}. In addition, other important design parameters are addressed, such as the shape of the primary mirrors, the receiver configuration, the collector length and the point strategy.

As reference case, the initial configuration of the LFR for this study was stablished following the

considerations previously detailed. This configuration consisted of 12 mirrors of 0.28 m wide, separated 0.14 m between them. From this starting point, the rest of features were optimized using the RTC.

3.1 *Concentrator optimization*

3.1.1 *Shape of primary mirrors*

As first step, a comparison of the power impinging on the receiver was performed between cylindrical and flat shaped mirrors (see section 2.2.1.1). An increase in the mirror width delivered an increment of the power in the receiver for both options, until mirrors reach the same width of the receiver. For mirror width higher than the receiver width, the increase of this parameter leads to directly enhance the power for the cylindrical shape. However, the flat shape does not respond with the same behavior because of the overflow effect previously explained. According to these results, the cylindrical shaped mirrors are preferred instead of flat shaped mirrors. Adding this result to the theoretical comparison between flat and parabolic mirrors reported in section 2.2.1.1, it can be concluded that flat mirrors are not suitable and may be dismissed.

Once the cylindrical shaped mirrors are preferred against parabolic ones due to economic reasons (see section 2.2.1.1), the next steps consist of selecting the proper radius of curvature form them. From an optical point of view, every mirror has a singular focal distance to the receiver, which leads to a different radius of curvature for each mirror. Manufacturing different preformed patterns with every radius of curvature certainly increases the cost of the LFR. An iteration process was performed with the goal of maximizing the power impinging in the receiver while using one single radius of curvature for all mirrors. At each iteration, a specific radius of curvature was employed for all mirrors, which was changing from the focal distance of the farthest mirrors from the receiver to the focal distance of the nearest one. It was established that the radius of curvature of the farthest mirror delivers the best results. In addition, it was concluded that the impinging power in the receiver for this particular configuration (i.e. the radius used for all the mirrors is the one corresponding to the farthest one) is similar to the power achieved when every mirror has its own specific radius (with an average difference of 2%).

3.1.2 *Concentrator tilt, λ*

The purpose was to find the optimal tilt, λ_{opt}, of the reflective surface and the receiver in the north-south direction. Fig. 7 shows the RTC results for the yearly normalized accumulated power (NAP) as a function of the tilt, λ, at the location considered for the case study, which is Tabernas desert in southern Spain (Latitude = 37.1°N, Longitude = 2.35°W), resulting a value of λ_{opt} equal to 25.8º. According to a geometrical approach, λ_{opt} should be in the neighboring of the latitude where the facility will be erected. However, as it can be seen in Fig. 7, λ_{opt} differs from the latitude of Tabernas-Almeria, because the optimization was performed taking into consideration the whole-year conditions. The influence of the time of the year when the Sun is near of the zenith leads to a lower value of λ_{opt}, yielding a more horizontal tilt of the plane containing reflectors' axes.

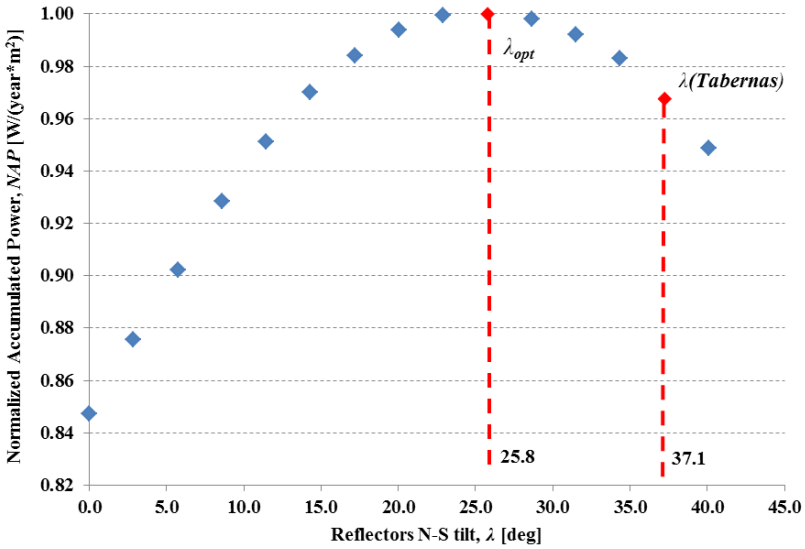

Fig. 7. Normalized Accumulated Power impinging on the receiver vs. reflector tilt, λ.

422

423 The value of λ_{opt} found implies that the northern side of the collector will be 5 m higher than the southern
424 side (considering the collector length calculated in section 3.2.1). This represents a difficult in terms of
425 accessibility for cleaning and maintenance altogether with and extra mechanical stress on the supporting
426 bearings as a consequence of the axial component of the weight. In order to minimize these setbacks, the
427 selected λ is smaller than the optimal. The settled value of λ is the one that allows an easily access to the
428 northern end of the collector and significates less efforts for the mechanical components. With this goal, λ
429 was fixed to λ_{Set} = 8.6º, which still represents an important improvement in terms of optical performance,
430 and means only 2 m of difference in height on the north-south axis.

431 As stated in the section 2.2.1.3., θ_L takes a major relevance in terms of the optical performance of the
432 collector. It was considered to be useful addressing the impact of the tilt in the reflective surface to
433 represent this phenomenon by comparing the three configurations, i.e., λ_{opt}, λ_{set} and horizontal tilt, λ_0, for
434 one representative day of every month of the year (see Fig. 8).

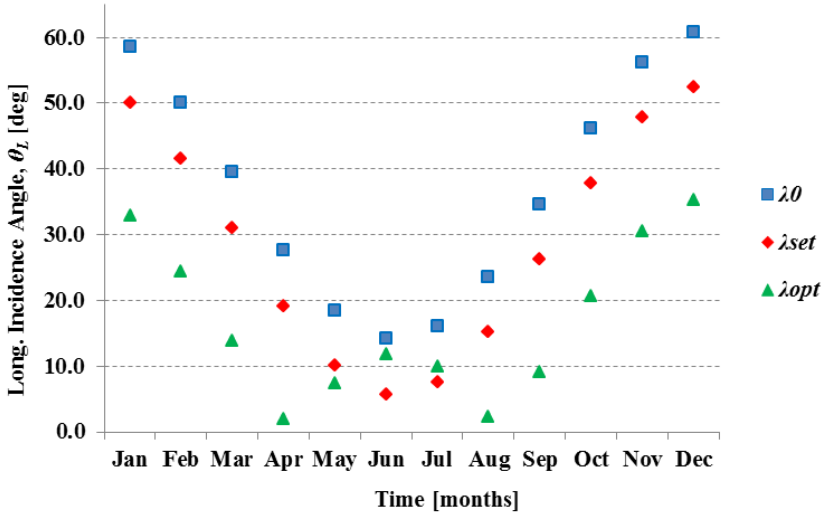

Fig. 8. Average longitudinal component of the incidence angle along a year for different reflector tilts

(λ_0, λ_{set} and λ_{opt}).

If λ_{opt} is considered (see Fig. 8), θ_L presents the smallest values for almost all the year, except for the month in which the Sun position is near of its zenith (that is, June and July). In these months the incidence angle raises its absolute value as a consequence of the pronounce tilt of the reflector surface. Nevertheless, in the months of January to May and August to December λ_{opt} represents a significant improvement in terms of optical performance. With respect to λ_{set}, the behavior of θ_L shows smaller value compared to λ_0 during the whole year, although not as effective as λ_{opt} for the periods from January to May and August to December. In addition, due to the reducer tilt compared with λ_{opt}, λ_{set} does not have the disadvantage of the months of June and July.

As it was mentioned in section 2.2.1.3., another enhancement provided by the tilt of the reflective surface is the shrink of the path of the reflected rays leaded from the mirrors to the receiver. As expected, it can be seen in Fig. 9 that the smallest distance traveled for the rays is reached with λ_{opt}. The main outcome of this analysis is the predominant effect in the reduction of the path with the reflector tilt, for the months with the highest θ_L (from January to March and from October to December). In these months the shrinking is more noticeable, which yields the homogenization of the optical performance along the whole year.

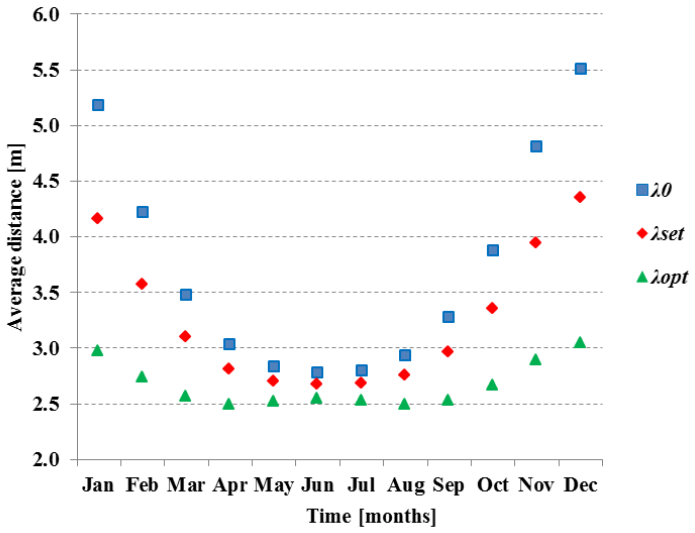

Fig. 9. Average distance traveled by the reflected rays from the mirrors to the receiver along the year for different reflector tilts (λ_0, λ_{set} and λ_{opt}).

3.1.3 *East-west concentrator rotation, β*

The optimum angle for the east-west concentrator rotation, β_{opt}, is the result of a calculation performed by the RTC at every change in the Sun position along the day. The code automatically computes θ (which is the angle of incidence, composed by the transversal and longitudinal incidence angles, θ_T and θ_L) between every reflector contained in the rotated set of mirrors and the incoming Sun ray, and then select the β_{opt} that find the average minimal θ at the given conditions. The influence of the east-west concentrator rotation in the NAP by months can be seen in Fig. 10, both for β_{opt} and β_0 (that is, horizontal). When β_{opt}

is adopted, the power impinging on the receiver is higher with respect to the cases without rotation. This modification implies an increment of 8.1% in the NAP. As it was detailed in section 2.2.1.4, this improvement is the result of the reduction of blocks and shadows between mirrors and the decrease of cosine factor related to the decrease of the θ in an average of 7.4% along the year (see Fig. 11).

In particular, the blocks and shadows effect could be accurately described by the amount of rays that are impinging in the receiver. This accounting was performed for several sun positions with high incidence angle, which are those for which the modification was designed. For example, comparing with a standard LFR design, the results showed an increment in the number of rays of 3% when the zenith angle of the sun is 60º and azimuth is 95º. If zenith angle is 80º and azimuth is 110º, the number of rays increases about 60%, (zenith is 0º in upper position and azimuth is 0º in the North).

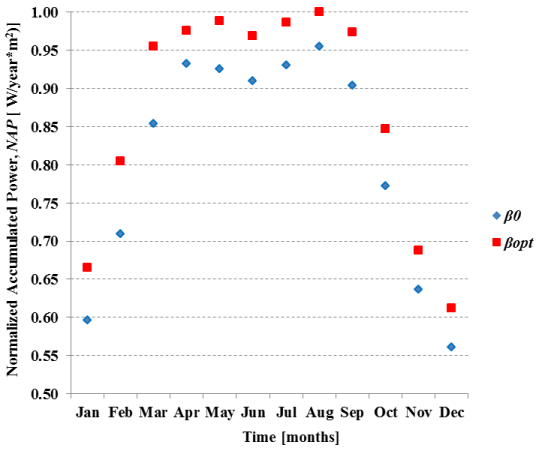

Fig. 10. Comparison of monthly normalized accumulated power for two concentrator rotation values (β_0 and β_{opt}).

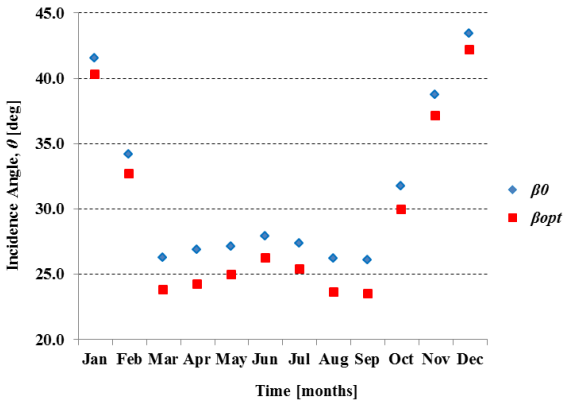

Fig. 11. Comparison of monthly average incidence angle for two concentrator rotation values (β_0 and β_{opt}).

3.2. *Receiver optimization*

3.2.1 *Receiver configuration and collector length*

The final receiver configuration selected was based on the information collected from the literature revision performed. A trapezoidal cavity with a multitube absorber and a glass window design presents the best optical performance and operational conditions in terms of flow control alongside the simplicity of the receiver assembly. After considering several configurations (ranging from 2 to 8 tubes), the design chosen incorporates six parallels tubes. This design is flexible and allows restricting the flow to central tubes, if radiation is lower than a certain value, in order to maintain a stable operating temperature. A central metallic structure, aligned in a north-south direction, holds the receiver. These metallic tubes (stainless steel or aluminum) are covered in its outer surface with a selective coating, which increases the absorption of concentrated sunlight and at the same time reduces heat losses on its surface by radiation to environment. All tubes are installed in parallel, so that its axial axis belongs to the same plane. The distance between the centers of two adjacent tubes is exactly twice of their outer radios. In this way, these contiguous tubes are in contact to avoid the concentrated radiation passing through this plane without intercepting them.

In line with the methodology explained in section 2.2.2.2, it has been considered as a design criterion a high Reynolds number, *Re*=4000, related with turbulent flow and a temperature increase of 20ºC. Additionally, a conservative value of overall efficiency was set, η=0.6 according to literature (Abbas, Montes, and Rovira 2016),finally the fluid properties at the working temperature where obtain from (Incropera et al. 2011). As a result of the former thermal balance, a total collector length of 10 m is proposed for this particular LFR design.

3.2.2 *Point strategy*

This section contains the simulation results considering two different point strategies, central point strategy or individual point strategy. Fig. 12 shows the image form by the rays if every mirror would point to the central position of the receiver. In this approach, the rays are concentrated in the central tubes, leaving the external tubes with no rays at all. As it was explained in section 2.2.2.3, this point strategy leads to generate hot spots that are counter-productive to the overall performance of LFR and may damage the absorber materials.

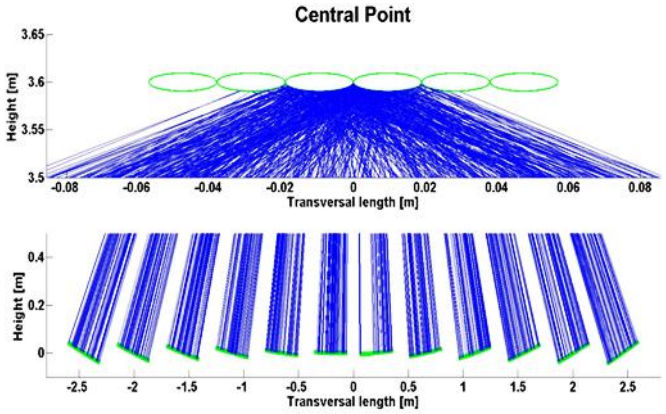

Fig. 12. Rays impinging on receiver following a central point strategy.

On the contrary, if an individual point strategy is taken into account, a group of mirrors aims exclusively at a specific tube or group of tubes. In this case, the image formed by the rays is noticeably homogeneously distributed, as expected. As it can be seen in Fig. 13, the power flux in the receiver is more uniform when this strategy is applied in comparison with the central point strategy. In this figure, the red lines represent those rays missing the receiver (that can be corrected by modifying the target of the external mirrors). The point strategy assumed in this case is based on a trade-off between the concentration ratio and flux distribution.

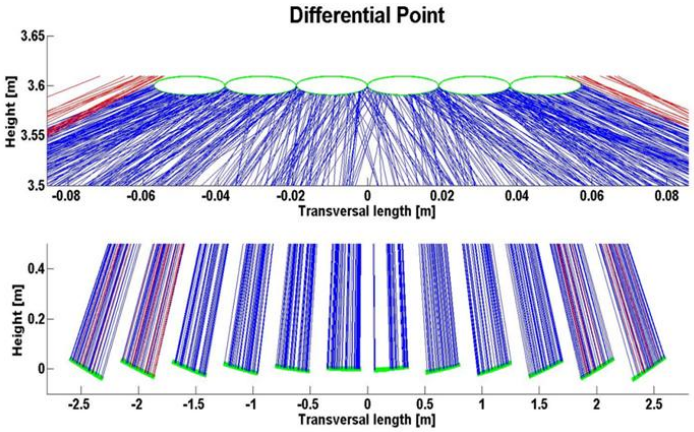

Fig. 13. Rays impinging in receiver following a differential point strategy.

3.2.3 *Receiver height, H*

Several simulations were done to compute the optimum receiver height, H_{opt}, by maximizing the power delivered to the receiver. Fig. 14 shows the NAP along the year for several heights of the receiver for a previously settled collector tilt, λ_{set}. It can be clearly seen from the numerical results that there is one specific value in which the power is maximized for this particular configuration, H_{opt}=2.3 m. However, there is certain flexibility to determinate H_{opt}, which might be adapted to the facility characteristics without jeopardizing the collected power. In this particular case, there is a range from 1.9 m to 2.5 m in which the behavior is relatively similar, implying just a variation less than 1%.

When the receiver is placed below the H_{opt}, blocking and shadows become predominant. Consequently, fewer rays reach the receiver, and therefore the impinging power is reduced. On the contrary, in case of locating the receiver above the optimal position, a higher rate of rays miss the target because the effect of sunshape becomes noticeable when the distance traveled by reflected rays increases.

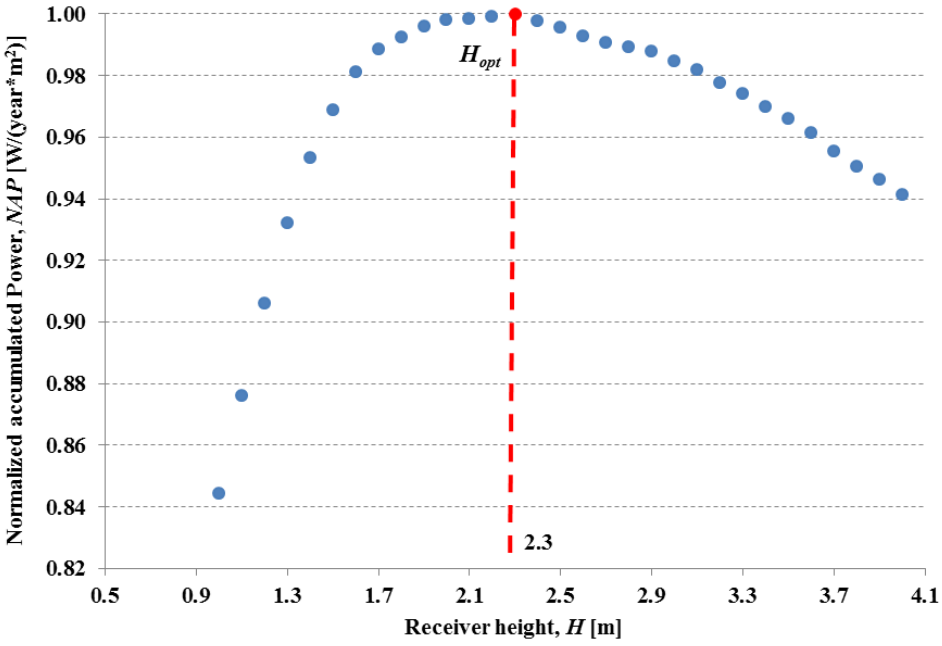

Fig. 14. Normalized accumulated power impinging on the receiver versus receiver height.

519 3.2.4 *Receiver displacement, dz*

520 The objective of the receiver displacement to the north direction in the longitudinal axis of the receiver
521 tubes (Fig. 3) is to intercept the rays that do not normally find the end of the receiver due to the Sun
522 position. Fig. 15 shows the optimal displacement, dz_{opt} that yields to maximize the NAP impinging in the
523 receiver along the year, for the three values of reflector tilt λ under consideration. For these three cases,
524 the increase of dz from zero yields to a higher NAP because the length of the tube displaced is collecting
525 the reflected rays that were missed at the collector end if no displacement were applied. This increase
526 reaches a maximum at dz_{opt}, corresponding to the length of the tube that compensates in average the end
527 losses along the year. For larger dz, the NAP decreases because the added receiver length at the collector
528 end is useless in the collection of the reflected rays, while the energy is being missed at its beginning.
529 Also, dz_{opt} is smaller when λ increases due to the decrease of the longitudinal component of the reflected
530 rays when the normal component of the reflective surface is higher. The value of dz_{opt} is 0.5 m when the
531 λ_{set} is set.

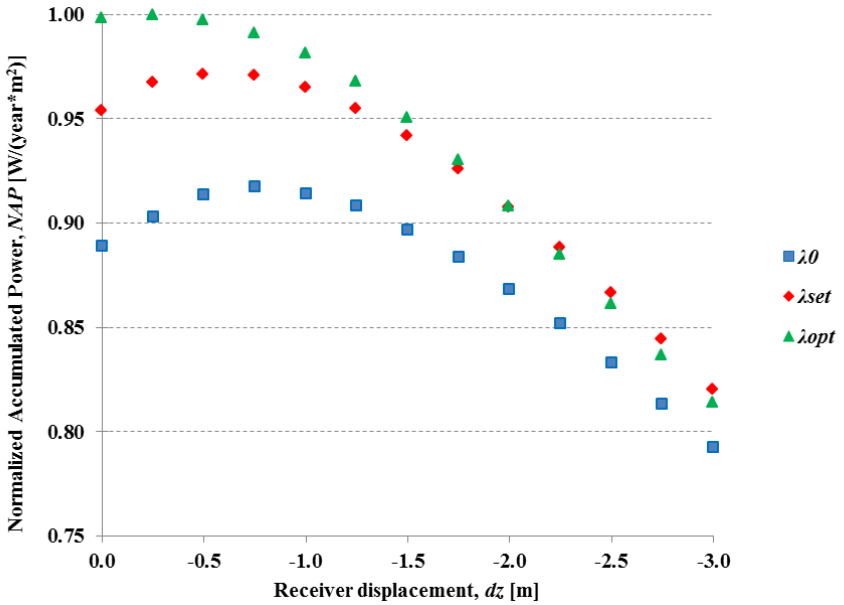

Fig. 15. Normalized accumulated power impinging on the receiver versus the receiver displacement, dz, for different reflector tilts (λ_0, λ_{Set} and λ_{Opt}).

532

533 **3.3 *Contribution of the modifications to the final design***

534 To visualize the contribution of each improvement proposed in this work, a comparison with a standard
535 configuration is done, taking into account λ_0, dz_0 and β_0. Table 1 summarizes the characteristics of the
536 standard design of LFR considered and the final design of the LFR set during the optimization process
537 described.

538 Table 1. Summary of modifications to the standard LFR configuration accomplished after the
539 optimization process

Parameter	Standard LFR	Optimized LFR

Number of mirrors [m]	12	12
Width of the mirrors [m]	0.28	0.28
Length of the mirrors [m]	Not defined	10
Receiver height, H [m]	Not defined	2.3
Concentrator tilt, λ [°]	0	8.6
Receiver displacement, dz [m]	0	0.5
East-west concentrator rotation, β [°]	0	Adjusted with sun position

3.3.1 Power production

Fig. 16 presents a bar graph with the monthly NAP for the different cases. The blue bars are the results for the standard design. The behavior along the year is the expected for a solar thermal collector, i.e., the trend of power production follows the accumulated DNI over the collector plane[†], which is also indicated in the graph. As can be observed, the month of July present an exceptional low DNI compared with the month of August and September, which is also reflected in the power production. In red color, the contribution of the north-south tilt of the reflective surface and receiver, λ_{set}, is shown. This is the most relevant advantage in terms of gained power. The displacement of the receiver, dz_{opt} is added to the previous contribution with the green bars. This adaptation takes importance for the months with higher incidence angles (from January to April and from September to December), while its contribution in the rest of the year is less relevant. Finally, in yellow color the contribution of the east-west rotation of the reflective surface, β_{opt}, is incorporated to the previous contributions. This one is the second in relevance and its performance along the year is quite steady.

"The most remarkable finding in this work, from the optical point of view expressed in terms of the NAP, is that the combination of all the modifications leads to homogenize the annual optical performance of the collector. This means that the increment of the power is most noticeable for the months with higher incidence angle. In particular, Fig. 16 shows that the increment of the NAP, compared to the optical performance of the collector without any of the modification performed is 61% in December and 53% in January and November, considering all the improvements proposed. On the other hand, those months with smaller incidence angle only present a slightly improve in the NAP, i.e., 8% in May, 2% in June and 5% in July. Considering the yearly contribution of each modification, the increment in NAP is 12.2% due to λ_{set}, when dz_{opt} is added raise up to 15.7% and finally, thanks to the incorporation of β_{opt}, the total enhancement of the NAP is 22.4%.

[†] It has been used a data set of a meteorological year collected at the *Plataforma Solar de Almeria.*

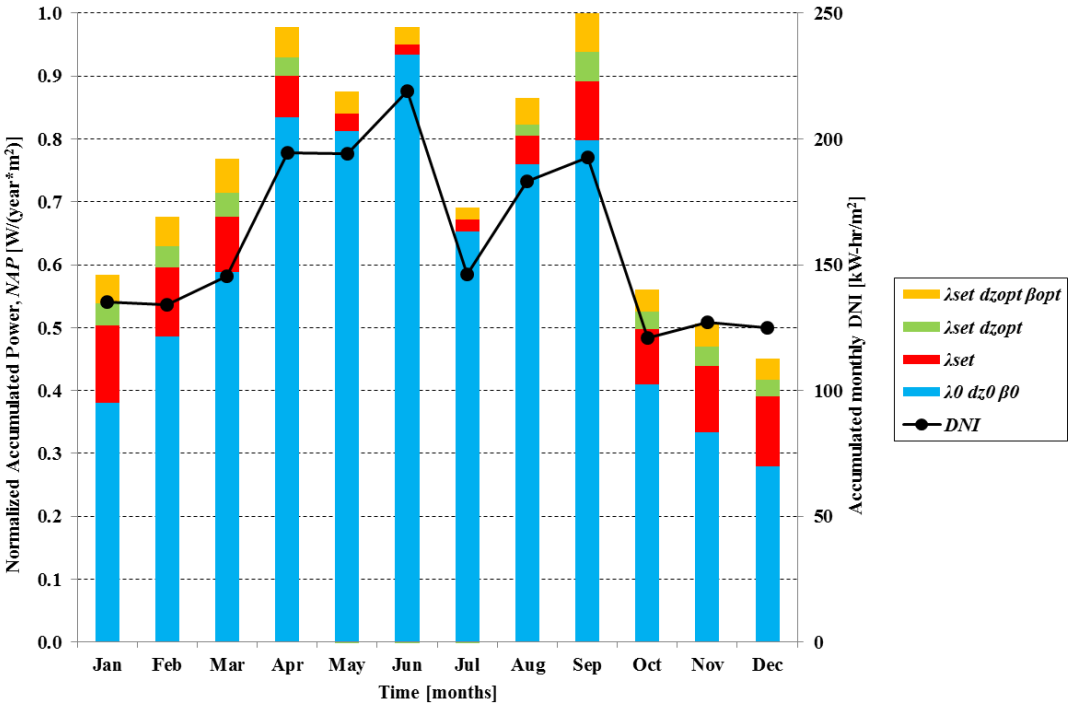

Fig. 16. Monthly distribution of the NAP for every modification and monthly accumulated DNI.

564

565 3.3.2 Incidence angle modifier

566 This section emphasizes the impact of the improvements to the design proposed in terms of the optical
567 behavior, by comparing the IAM considering the modifications proposed with respect to the basis
568 configuration of the collector. Fig. 17 shows the IAM for a standard design, which means λ_0, dz_0 *and* β_0,
569 while Fig. 18 presents the IAM for a LFR with the optimization of the key parameters explained above
570 (λ_{set}, dz_{opt} *and* β_{opt}). It might be observed in both figures, that when sun altitude decreases (zenith
571 increases) a noticeable reduction of the IAM is achieved while the change of the IAM when the
572 transversal angle (azimuth) is moved is significantly smoother.

573 It can be remarked that for the standard configuration (see Fig. 17) the IAM reaches its maximum of 1 for
574 the combination of 180° azimuth and 0° zenith. This is the expected behavior when a horizontal surface is
575 receiving radiation from the Sun at its upper position (0° zenith and noon).

576 With respect to the optimized LFR design (see Fig. 18), the influence of these modifications is clear in
577 terms of the displacement of the maximum IAM, reaching the higher value of 1 for 180° azimuth and 15°
578 zenith. As λ_{set} was set at 8.5°, it could be expected that the maximum IAM takes place when the zenith
579 angle is λ_{set}. However, the influence of the receiver displacement, dz_{opt}, involves that the maximum IAM
580 appears when zenith angle is higher than the expected one. This could be explained by the fact that for
581 perpendicular interaction between the Sun and the collector, the rays that impinge in the south area of the
582 LFR aperture will miss the receiver, because this was displaced northern. And thus, the optimal position
583 is reached when the Sun is lower and reflected rays have some south component.

584 Comparing both figures, the impact of the modifications applied is noticeable because higher IAM values
585 are achieved in the optimized configuration for every Sun position. The former leads to emphasize the
586 advantages of the propose LFR design related to the optical performance.

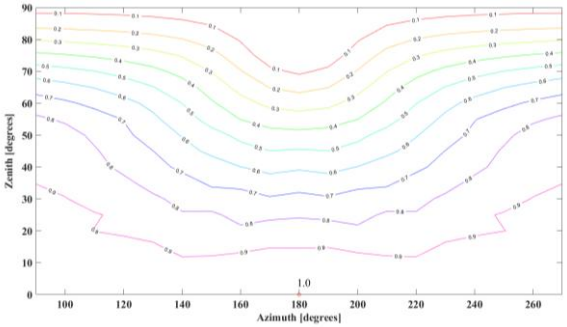

Fig. 17. IAM for the standard parameters, λ_0, dz_0 *and* β_0

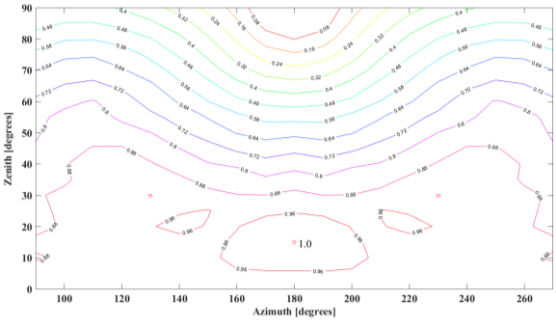

Fig. 18. IAM for the optimized parameters, λ_{set}, dz_{opt} *and* β_{opt}

587

588 Finally is worth to mention that the proposed design has been accept into the patent process, the
589 registration number is PCT/ES2018/070059.

590 **4. Conclusions**

591 An innovative linear Fresnel collector to supply heat in industrial processes is designed and optimized for
592 the location of the *Plataforma Solar de Almería* (Spain), by using an optimization tool based on optical
593 ray-trace technique. The improvements incorporated to the new design of collector provide significant
594 advantages over conventional LFRs. It is a compact and unique design with fixed collector length, so that
595 the system is fully scalable if it is needed higher thermal power than the provided by a single module.
596 Although the results presented are particular for the case study considered, the concept proposed is
597 feasible in a wide range of geographical latitudes.

598 The proposed configuration of LFR comprises different geometrical modifications. First, the shape of the
599 primary mirrors was stablished as cylindrical. This involves higher concentration ratio compared with flat
600 mirrors, besides cylindrical mirrors are easier to be manufactured than parabolic ones. It was proved that
601 a tilt in the receiver and concentrator improves the optical performance related with the influence of the
602 incidence angle. A suitable tilt was found, taking into consideration an optimum value and some technical
603 constraints. Another innovation was in east-west concentrator rotation system, which leads enhanced
604 optical efficiency because shadowing and blocking effects are reduced. The optimum rotation that
605 maximizes the normalized accumulated power impinging on the receiver of the LFR was calculated.
606 Relative to the receiver, it was chosen a trapezoidal cavity with multitube absorber configuration. The
607 aiming strategy followed was the one named differential point, which delivers a homogenous solar flux
608 on the receiver and avoid hot spots. The optimal receiver height that maximizes the accumulated power
609 was found. This is the only parameter that does not need an accurate adjustment because it involves
610 similar optical behavior for a wide range of values of receiver heights. Finally, it was demonstrated that
611 the receiver displacement counteracts the effect of end losses, existing an optimum value.

The set of changes proposed in this work results in an important increase in the optical performance of the collector along the whole year and, consequently, in the thermal power delivered to any industrial process. The most relevant advantage in terms of power gained is the tilt of the collector and receiver. The improvement is more significant in the months with lower Sun altitude, which causes a more homogeneous power along the year. All this progress was backed up for the noticeable improvement of the optical performances related with the IAM.

Acknowledgements

The first author thanks to Universidad de Antofagasta (Chile) for the funds received to realize his PhD studies at *Plataforma Solar de Almería* and *Universidad de Almería*. This work has been developed under the framework of the Spanish Project SOLTERMIN (Grant no. ENE2017-83973-R) supported by the *Programa Estatal de Investigación, Desarrollo e Innovación orientada a los Retos de la Sociedad* (National Program of Research, Development and Innovation oriented to Society's Challenges) of the *Ministerio de Economía y Competitividad* (Spanish Ministry of Economy and Competitiveness). Additionally, the research leading to this work has also received funding from the EU Horizon 2020 – H2020-LCE-2016-2017 under grant agreement n° 731287 (Integrating National Research Agendas on Solar Heat for Industrial Processes, INSHIP).

References

Abbas, R., J. Muñoz-Antón, M. Valdés, and J. M. Martínez-Val. 2013. "High Concentration Linear Fresnel Reflectors." *Energy Conversion and Management* 72. Elsevier Ltd: 60–68. doi:10.1016/j.enconman.2013.01.039.

Abbas, R., J. Muñoz, and J. M. Martínez-Val. 2012. "Steady-State Thermal Analysis of an Innovative Receiver for Linear Fresnel Reflectors." *Applied Energy* 92. Elsevier Ltd: 503–15. doi:10.1016/j.apenergy.2011.11.070.

Abbas, R. 2017. "A Comprehensive Optical Characterization of Linear Fresnel Collectors by Means of an Analytic Study." *Applied Energy* 185: 1136–51.

Abbas, R, M J Montes, and A Rovira. 2016. "Parabolic Trough Collector or Linear Fresnel Collector ? A Comparison of Optical Features Including Thermal Quality Based on Commercial Solutions." *Solar Energy* 124: 198–215.

Azofra, D, E Martínez, E Jiménez, J Blanco, and J C Saenz-díez. 2014. "Comparison of the Influence of Biomass , Solar – Thermal and Small Hydraulic Power on the Spanish Electricity Prices by Means of Artificial Intelligence Techniques." *Applied Energy* 121: 28–37.

Barbon, A., Barbon, N., Bayon, L. 2016. "Optimization of the Length and Position of the Absorber Tube in Small-Scale Linear Fresnel Concentrators" 99: 986–95. doi:10.1016/j.renene.2016.07.070.

Bermejo, Pablo, Francisco Javier Pino, and Felipe Rosa. 2010. "Solar Absorption Cooling Plant in Seville." *Solar Energy* 84 (8). Elsevier Ltd: 1503–12. doi:10.1016/j.solener.2010.05.012.

Bernhard, Rolf, Hg Laabs, and Jacques De Lalaing. 2008. "Linear Fresnel Collector Demonstration on the PSA, Part I–design, Construction and Quality Control." In *SolarPaces Conference*. http://www.researchgate.net/publication/225000351_Linear_Fresnel_Collector_Demonstration_on_the_PSA_Part_I__Design_Construction_and_Quality_Control/file/60b7d515e950a285ce.pdf.

Blanco, Manuel J, Amaia Mutuberria, Pierre Garcia, Raquel Gastesi, and Victor Martin. 2009. "Preliminary Validation of Tonatiuh." In *SolarPaces Conference*.

Boito, Paola, and Roberto Grena. 2016. "Optimization of the Geometry of Fresnel Linear Collectors." *Solar Energy* 135. Elsevier Ltd: 479–86. doi:10.1016/j.solener.2016.05.060.

Buie, D., C. J. Dey, and S Bosi. 2003. "The Effective Size of the Solar Cone for Solar Concentrating Systems." *Solar Energy* 74 (5): 417–27.

Buie, D., A. G. Monger, and C. J. Dey. 2003. "Sunshape Distributions for Terrestrial Solar Simulations." *Solar Energy* 74 (2): 113–22. doi:10.1016/S0038-092X(03)00125-7.

Corona, B., E. Cerrajero, D. López, and G. San Miguel. 2016. "Full Environmental Life Cycle Cost Analysis of Concentrating Solar Power Technology: Contribution of Externalities to Overall Energy Costs." *Solar Energy* 135. Elsevier Ltd: 758–68. doi:10.1016/j.solener.2016.06.059.

Dai, Jing, Hongfei Zheng, Yuehong Su, and Zehui Chang. 2012. "Energy Procedia The Motional Design and Analysis for Linear Fresnel Reflector System Combined Three-Movement" 14: 971–76.

664 doi:10.1016/j.egypro.2011.12.1041.

665 European Comission. 2017. “Paris Agreement.” *Climate Action*.
666 https://ec.europa.eu/clima/policies/international/negotiations/paris_en.

667 Freeman, James, Klaus Hellgardt, and Christos N. Markides. 2015. “An Assessment of Solar–Thermal
668 Collector Designs for Small-Scale Combined Heating and Power Applications in the United
669 Kingdom.” *Heat Transfer Engineering* 36 (14–15): 1332–47. doi:10.1080/01457632.2015.995037.

670 García-Rodríguez, Lourdes, and Julián Blanco-Gálvez. 2007. “Solar-Heated Rankine Cycles for Water
671 and Electricity Production: POWERSOL Project.” *Desalination* 212 (1–3): 311–18.
672 doi:10.1016/j.desal.2006.08.015.

673 Güven, H. M., and R. B. Bannerot. 1986. “Determination of Error Tolerances for the Optical Design of
674 Parabolic Troughs for Developing Countries.” *Solar Energy* 36 (6): 535–50.

675 Häberle, Andreas, Michael Berger, Frank Luginsland, Christian Zahler, Michael Baitsch, Hans-Martin
676 Henning, and Matthias Rommel. 2006. “Linear Concentrating Fresnel Collectors.” In *SolarPaces*
677 *Conference*, 1–8.

678 Häberle, Andreas, Christian Zahler, Hansjoerg Lerchenmueller, Max Mertins, Christof Wittwer, Franz
679 Trieb, and Juergen Dersch. 2002. “The Solarmundo Line Focussing Fresnel Collector. Optical and
680 Thermal Performance and Cost Calculations.” In *SolarPaces Conference*.

681 Huang, Farong, Longlong Li, and Weidong Huang. 2014. “Optical Performance of an Azimuth Tracking
682 Linear Fresnel Solar Concentrator.” *Solar Energy* 108. Elsevier Ltd: 1–12.
683 doi:10.1016/j.solener.2014.06.028.

684 IEA. 2016. “Key World Energy Statistics 2016.” *Statistics*, 80. doi:10.1787/9789264039537-en.

685 Incropera, Frank P., David P. DeWitt, Theodore L. Bergman, and Lavine S. Adrianne. 2011.
686 *Fundamental of Heat and Mass Transfer*. 7th ed. New York: John Wiley & Sons.

687 Inersur. 2017. “Inersur.” http://www.inersur.com/.

688 Matsumoto, M, and T Nishimura. 1998. “Mersenne Twister: A 623-Dimensionally Equidistributed
689 Uniform Pseudorandom Number Generator.” *ACM-Trans. on Modeling and Computer Simulation* 8
690 (1): 3–30.

691 Millioud, A, and J Dreyer. 2008. “074 - Novel Parabolic Trough Collector for Roof Mounted Solar
692 Cooling Applications.” *Eurosun 2008*, 1–8.

693 Mokhtar, Ghodbane, Boumeddane Boussad, and Said Noureddine. 2016. “A Linear Fresnel Reflector as a
694 Solar System for Heating Water: Theoretical and Experimental Study.” *Case Studies in Thermal*
695 *Engineering* 8 (August 2010). Elsevier: 176–86. doi:10.1016/j.csite.2016.06.006.

696 Mokhtar, Marwan, Michael Berger, Christian Zahler, and Dirk Krüger. 2015. “Direct Steam Generation
697 for Process Heat Using Fresnel Collectors.” *Int. J. of Thermal & Environmental Engineering* 10 (1):
698 3–9. doi:10.5383/ijtee.10.01.001.

699 Montes, María J, Rubén Barbero, Rubén Abbas, and Antonio Rovira. 2016. “Performance Model and
700 Thermal Comparison of Different Alternatives for the Fresnel Single-Tube Receiver.” *Applied*
701 *Thermal Engineering* 104: 162–75.

702 Morin, Gabriel, Max Mertins, Jann Kirchberger, and Martin Selig. 2011. “SUPERNOVA – Construction,
703 Control & Performance of Steam Superheating Linear Fresnel Collector.” In *SolarPaces*
704 *Conference*.

705 NEP Solar. 2018. “NEP SOLAR.” http://www.nep-solar.com/.

706 Nixon, J. D., and P. A. Davies. 2016. “Construction and Experimental Study of an Elevation Linear
707 Fresnel Reflector.” *Journal of Solar Energy Engineering* 138 (3): 031001. doi:10.1115/1.4032682.

708 Qiu, Yu, Ya-ling He, Ze-dong Cheng, and Kun Wang. 2015. “Study on Optical and Thermal Performance
709 of a Linear Fresnel Solar Reflector Using Molten Salt as HTF with MCRT and FVM Methods.”
710 *Applied Energy* 146: 162–73.

711 REN21. 2016. “Energías Renovables 2016 Reporte De La Situación Mundial,” 8–12.

712 Sahoo, Sudhansu S, Suneet Singh, and Rangan Banerjee. 2012. “Analysis of Heat Losses from a
713 Trapezoidal Cavity Used for Linear Fresnel Reflector System.” *Solar Energy* 86: 1313–22.
714 doi:10.1016/j.solener.2012.01.023.

715 Sait, Hani H., Jose M. Martinez-Val, Ruben Abbas, and Javier Munoz-Anton. 2015. “Fresnel-Based
716 Modular Solar Fields for Performance/Cost Optimization in Solar Thermal Power Plants: A
717 Comparison with Parabolic Trough Collectors.” *Applied Energy* 141. Elsevier Ltd: 175–89.
718 doi:10.1016/j.apenergy.2014.11.074.

719 Selig, Martin. 2011. “Commercial CSP Plants Based on Fresnel Collector Technology.” In *SolarPaces*
720 *Conference*.

721 Solatom. 2017. “Solatom.” http://solatom.com/.

722 Tierney, M. J. 2007. “Options for Solar-Assisted Refrigeration-Trough Collectors and Double-Effect
723 Chillers.” *Renewable Energy* 32 (2): 183–99. doi:10.1016/j.renene.2006.01.018.

724 Vannoni, Claudia., David R. Tobergte, and Shirley Curtis. 2013. “Potential for Solar Hear in Industrial
725 Processes.” *Journal of Chemical Information and Modeling* 53 (9): 1689–99.
726 doi:10.1017/CBO9781107415324.004.

727 Wang, Fu, Jun Zhao, Hailong Li, Shuai Deng, and Jinyue Yan. 2017. “Preliminary Experimental Study of
728 Post-Combustion Carbon Capture Integrated with Solar Thermal Collectors.” *Applied Energy* 185.
729 Elsevier Ltd: 1471–80. doi:10.1016/j.apenergy.2016.02.040.

730 Werner, Sven, and Norela Constantinescu. 2006. “N. ECOHEATCOOL, The European Heat Market.”

731 Yanqing, Zhu, Shi Jifu, Li Yujian, Wang Leilei, Huang Qizhang, and Xu Gang. 2016. “Design and
732 Experimental Investigation of a Stretched Parabolic Linear Fresnel Reflector Collecting System.”
733 *Energy Conversion and Management* 126. Elsevier Ltd: 89–98.
734 doi:10.1016/j.enconman.2016.07.073.

735 Zhu, Guangdong. 2013. “Development of an Analytical Optical Method for Linear Fresnel Collectors.”
736 *Solar Energy* 94. Elsevier Ltd: 240–52. doi:10.1016/j.solener.2013.05.003.

737 Zhu, Yanqing, Jifu Shi, Yujian Li, Leilei Wang, Qizhang Huang, and Gang Xu. 2017. “Design and
738 Thermal Performances of a Scalable Linear Fresnel Reflector Solar System.” *Energy Conversion*
739 *and Management* 146. Elsevier Ltd: 174–81. doi:10.1016/j.enconman.2017.05.031.

740